INL/CON-13-30395
PREPRINT

Comparison of the PHISICS/RELAP5-3D Ring and Block Model Results for Phase I of the OECD MHTGR-350 Benchmark

ICAPP 2014

Gerhard Strydom

April 2014

The INL is a
U.S. Department of Energy
National Laboratory
operated by
Battelle Energy Alliance

Proceedings of ICAPP 2014
Charlotte, USA, April 6-9, 2014
Paper 14272

Comparison of the PHISICS/RELAP5-3D Ring and Block Model Results for Phase I of the OECD MHTGR-350 Benchmark

Gerhard Strydom
Idaho National Laboratory
2525 N. Fremont Avenue, Idaho Falls, Idaho 83415
Tel: (208) 526-1216, Fax: (208) 526-2930, Email:gerhard.strydom@inl.gov

Abstract – *The INL PHISICS code system consists of three modules providing improved core simulation capability: INSTANT (performing 3D nodal transport core calculations), MRTAU (depletion and decay heat generation) and a perturbation/mixer module. Coupling of the PHISICS code suite to the thermal hydraulics system code RELAP5-3D has recently been finalized, and as part of the code verification and validation program the exercises defined for Phase I of the OECD/NEA MHTGR 350 MW Benchmark were completed. This paper provides an overview of the MHTGR Benchmark, and presents selected results of the three steady state exercises 1-3 defined for Phase I. For Exercise 1, a stand-alone steady-state neutronics solution for an End of Equilibrium Cycle Modular High Temperature Reactor (MHTGR) was calculated with INSTANT, using the provided geometry, material descriptions, and detailed cross-section libraries. Exercise 2 required the modeling of a stand-alone thermal fluids solution. The RELAP5-3D results of four sub-cases are discussed, consisting of various combinations of coolant bypass flows and material thermophysical properties. Exercise 3 combined the first two exercises in a coupled neutronics and thermal fluids solution, and the coupled code suite PHISICS/RELAP5-3D was used to calculate the results of two sub-cases. The main focus of the paper is a comparison of the traditional RELAP5-3D "ring" model approach vs. a much more detailed model that include kinetics feedback on individual block level and thermal feedbacks on a triangular sub-mesh. The higher fidelity of the block model is illustrated with comparison results on the temperature, power density and flux distributions, and the typical under-predictions produced by the ring model approach are highlighted.*

I. INTRODUCTION

The Very High Temperature Reactor (VHTR) Code and Simulation Methods group at the Idaho National Laboratory (INL) leads the development of the Organization for Economic Cooperation and Development (OECD) MHTGR-350 Transient Benchmark for evaluating prismatic High Temperature Gas-Cooled Reactor (HTGR) analysis codes. The benchmark is sponsored by the OECD's Nuclear Energy Agency, and the project will eventually yield a set of peer-reviewed steady-state, transient, and lattice solutions that can be used by the Department of Energy, Nuclear Regulatory Commission and vendors to assess their codes. The technical specification is based on the General Atomics 350 MW Modular High Temperature Gas-Cooled Reactor (MHTGR) design [1]. The Methods group at INL is responsible for defining the benchmark specifications, lead the data collection and comparison activities, and chair the annual technical workshops. Several code development and verification activities from participants in Germany, Korea and the United States are currently based on the MHTGR-350 benchmark, and two conference publications on the INL progress have already been completed in 2012 [2],[3].

As part of the benchmark simulation activities, the Parallel and Highly Innovative Simulation for INL Code System (PHISICS) reactor physics package was coupled to the INL-developed system thermal analyses code RELAP5-3D to enable temperature feedback in coupled core simulations [3]. RELAP5-3D typically does not provide the spatial resolution of higher fidelity thermal fluid codes but it does have a well-validated plant simulation capability.

This paper summarizes the final INL results obtained for Phase I of the benchmark, with a specific focus on a comparison of the traditional homogenized (ring) model approach with a much more detailed triangular geometry model. These two models were developed during the coupling of the PHISICS/RELAP5-3D system to

investigate the effect of spatial refinements in the flux and temperature fields on the typical parameters of interest (fuel temperatures, keff), and to assess the suitability of utilizing a systems code like RELAP5-3D to provide more detailed temperature profiles.

II. MHTGR-350 BENCHMARK OVERVIEW

The MHTGR-350 MW benchmark specification was developed in cooperation with General Atomics to compare different codes and methods, since validation data from current or past prismatic HTGR experimental facilities or reactors are severely limited. The scope of the benchmark is to establish a well-defined problem based on a common given data set, and to compare methods and tools in core simulation and thermal hydraulic analysis through a set of multi-dimensional computational test problems. The benchmark consist of three Phase I steady-state exercises (summarized below), four Phase II transient exercises, and a single Phase III depletion exercise [1].

- **Exercise 1:** Neutronics only steady-state solution for the 350 MW End of Equilibrium Cycle (EOEC) MHTGR core, using the provided geometry, material descriptions, and detailed cross-section libraries.
- **Exercise 2:** Thermal hydraulics only steady-state core solution. Four sub-cases are defined, depending on the core bypass flow type and the use of fixed or variable thermophysical material properties. Participants are expected to provide steady-state solutions for each of these sub-cases according to their codes' capabilities. A defined core power distribution map must be used, since no neutronics are involved in this exercise.
- **Exercise 3:** Coupled neutronics-thermal hydraulic core steady state. This exercise is a combination the first two exercises and the coupled steady-state solution must be calculated using the provided temperature dependent cross-section library, burnup, and fluence distributions.

The radial and axial core layouts of the MHTGR-350 design are shown in Fig. 1 and Fig. 2, respectively, and the major core characteristics are summarized in Table I.

TABLE I

MHTGR-350 main characteristics

Description	
Power	350 MW(t)/165 MW(e)
Core/fuel design	Graphite moderated. 660 prismatic hex-blocks with 15.5 wt% enriched UCO TRISO fuel compacts.
Coolant	Helium @ 6.39 MPa
Core inlet/outlet gas temperature	259°C / 687°C

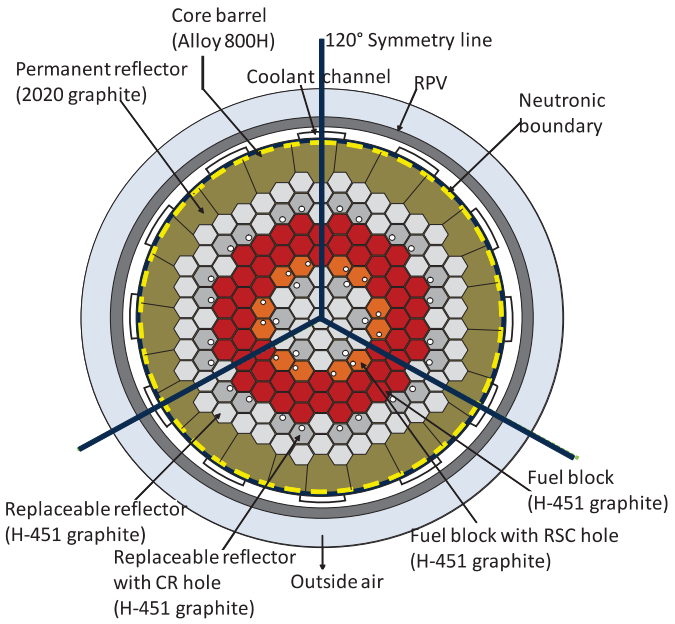

Fig. 1. MHTGR-350 core radial layout.

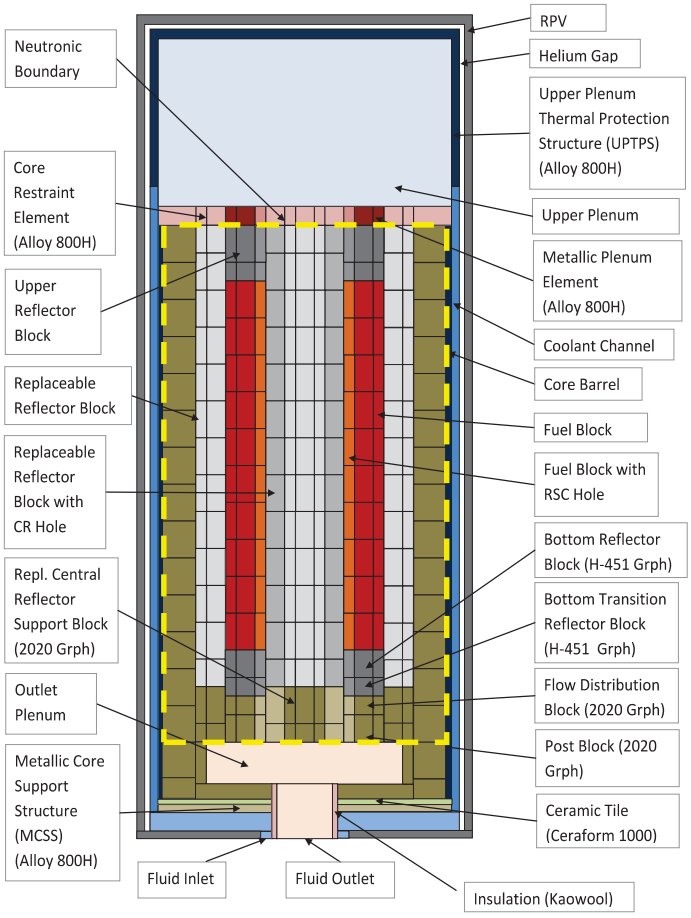

Fig. 2. MHTGR-350 core axial layout.

The 1/3rd core numbering utilized for the benchmark data reporting, and the discussion that follows in this paper, is shown in Fig. 3.

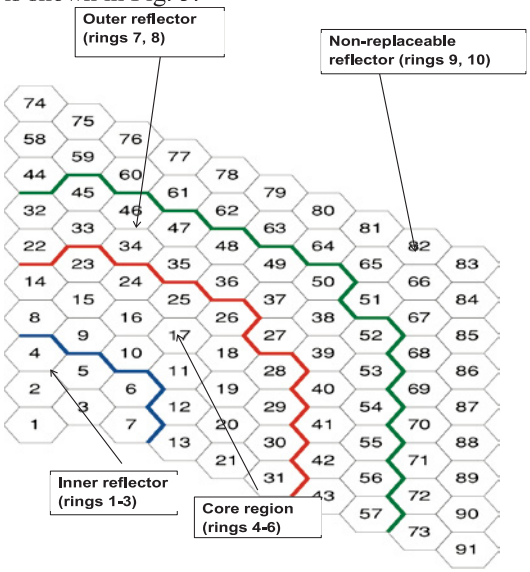

Fig. 3. Core numbering layout (axial layer 1).

III. CODE AND MODEL DESCRIPTION

III.A. PHISICS/RELAP5-3D Overview

The simulation of complex phenomena for advanced reactors such as Generation IV systems poses a challenge to existing thermal fluid system codes like RELAP5-3D [4]. For the analysis of the MHTGR-350 design more advanced neutronic capabilities are required compared to the available NESTLE neutronics package in RELAP5-3D, since the benchmark specifies the use of 26 energy groups (NESTLE is limited to four groups). The RELAP5-3D code was developed at INL for best-estimate transient simulation of LWRs, and the code is able to model coupled behavior of the reactor core and the secondary system of the power plant [5]. During the development planning of the coupling of PHISICS to RELAP5-3D, it was decided to couple the different modules of PHISICS directly to RELAP5-3D, i.e. PHISICS is integrated in RELAP5-3D as a set of subroutines.

PHISICS is a time-dependent neutronics code system developed at INL [5], and consists of three modules: a nodal spherical harmonics transport core solver (INSTANT [6]), a depletion module (MRTAU) and a cross-section mixer-interpolator (MIXER) module. The INSTANT transport solver is parallelized and based on the second order formulation of the transport equation discretized in angle by spherical harmonics while in space it uses orthonormal polynomials of an arbitrary order. A time-dependent scheme has recently been implemented as a new module for the PHISICS suite, based on a second order backward Euler scheme with explicit delayed neutron treatment [5]. MRTAU (Multi-Reactor Transmutation Analysis Utility) is a generic depletion code developed at INL [7]. The code tracks the time evolution of the isotopic concentration of a given material, and utilizes a Taylor series expansion based algorithm of arbitrary order and the Chebyshev Rational Approximation Method for computation of the exponential matrix. This module is utilized in Ex. 3 to calculate the equilibrium xenon concentration. The MIXER module performs all the cross-section handling for the different kernels. This module can treat macroscopic, microscopic, and "mixed" cross sections. More detailed descriptions of the PHISICS/RELAP5-3D coupling methodology can be found in [3] and [5].

III.B. Ring and Block Model Descriptions

Two PHISICS/RELAP5-3D models were developed for the benchmark. The "ring" model followed the widely-used system-code homogenization approach of modeling the inner reflector, fuelled core region, and outer reflector as nine rings in cylindrical coordinates, with three additional rings representing the core barrel (CB), reactor pressure vessel (RPV), and outer air boundary layer (Fig. 4). (The benchmark does not require the modeling of the MHTGR secondary system). Each of these rings is connected to its own heat structure representing fuel or graphite blocks on each axial level. The coarse axial mesh is discretized in 2 upper reflector, 10 core and 2 lower reflector elements, as shown in Fig. 2.

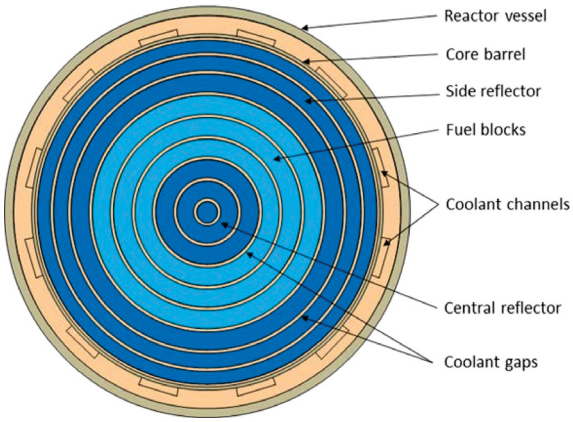

Fig. 4. "Ring" model radial representation.

The RELAP5-3D hydrodynamic nodalization is presented in Fig. 5. The time-dependent junction (#255) adjusts the inflow helium mass flow rate to obtain a target outlet helium temperature of 687°C through a control variable that combines the outlet pressure (6.39 MPa), inlet helium temperature (259°C) and the total thermal power (350 MW) boundary conditions. In addition to the core

region (component numbers 130-166), the model includes the lower plenum (110), coolant riser (115), upper plenum (120), outlet plenum (175), vessel gap (105) and outlet boundary condition (299) components.

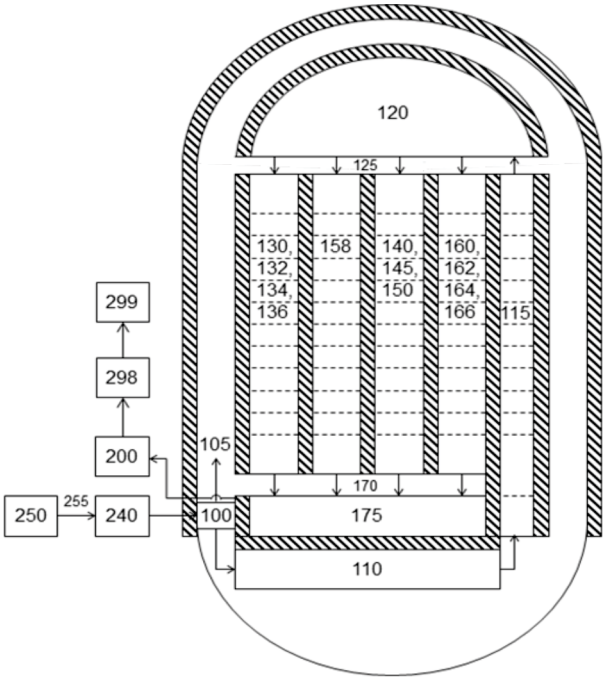

Fig. 5. RELAP5-3D ring model hydrodynamic nodalization.

The main helium flow through the three core rings is modeled as three 1-D pipes, and a total of seven core bypass flow channels through the 2mm gaps between the graphite blocks are as part of the 1-D hydrodynamics flow network, according to the specifications of the benchmark.

A number of conduction and radiation sets are included in the model to account for radial conduction and axial radiation between the graphite structures in the inner, outer, top and bottom reflectors. Radial radiation heat transfer is also modeled between the outer reflector surface and the core barrel, and from the outer surface of the reactor vessel to the boundary air layer. Adiabatic boundary conditions are applied at the top and bottom model boundaries, and the outer radial air layer is defined to be at a constant temperature of 30°C.

A sub-channel "unit-cell" approach is utilized for the three fuel rings to distinguish between the fuel and moderator temperatures. The cylindrical unit cell consists of a fuel compact, its surrounding matrix graphite and a helium coolant channel (Fig. 6). This homogenized unit cell can be utilized in two spatial representations of the core geometry; the traditional "ring" model described above, or a much more detailed "block" model.

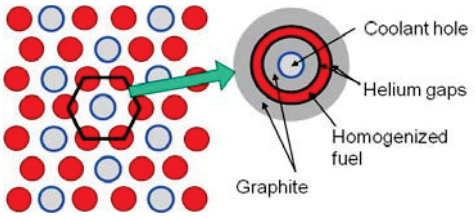

Fig. 6. Unit-cell configuration.

In the block model, a single hexagonal block can be explicitly represented by dividing it into six triangular elements, as shown in Fig. 7. Each of these block faces can be connected to a RELAP5-3D pipe element that provides the helium mass flow rates, velocities, and temperatures along the axial height of the core. The corresponding triangular RELAP5-3D heat structure region connected to this pipe provides the heat source information in the case of the core fuel blocks.

Heat transfer between the triangular elements occurs in two ways: inside a block via conduction, and between blocks via radiation across the 2 mm gap between the block faces. These connections are defined as part of the conduction and radiation enclosure sets in the RELAP5-3D model, in addition to the existing enclosure sets already defined for the ring model (as described above). This "block" model can therefore provide a much more detailed temperature distribution compared to the ring model shown in Fig. 4. In the case of the first fuel ring, for example, blocks 8-13 in Fig. 3 can now be represented with 6*6=36 triangular elements per axial layer, which provides 36 data points compared to only one value for the ring model.

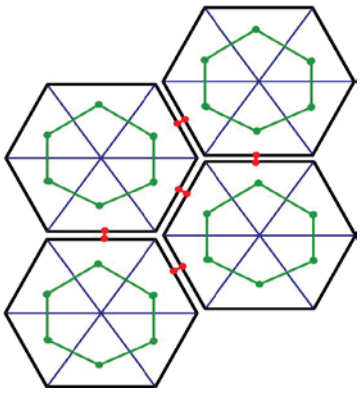

Fig. 7. Block model conduction and radiation connections.

For Ex. 2 of Phase I, a fixed power density was defined for each fuel block, but the modeling of Ex. 3 required the use of kinetic feedback zones to manage the exchange of power (calculated by INSTANT) and temperature (RELAP5-3D) data. There is however a limit on the number of these data types that the code can process.

A further RELAP5-3D restriction also requires that the left or right side of a heat structure can only be included in one type of enclosure, i.e. the left side of a triangular region cannot be connected to a conduction and radiation enclosure simultaneously. It was therefore decided to focus the RELAP5-3D triangular sub-division on the important regions of the active core region (Rings 4-6) and the two reflector rings next to the core (Rings 3 and 7).

The RELAP5-3D block model (Fig. 8) therefore consists of the "smeared-out" representation in Rings 1 and 2 (Blocks 1-3) and 8-10 (Blocks 44-91), and a detailed triangular resolution in Rings 3-7 (Blocks 8-43).

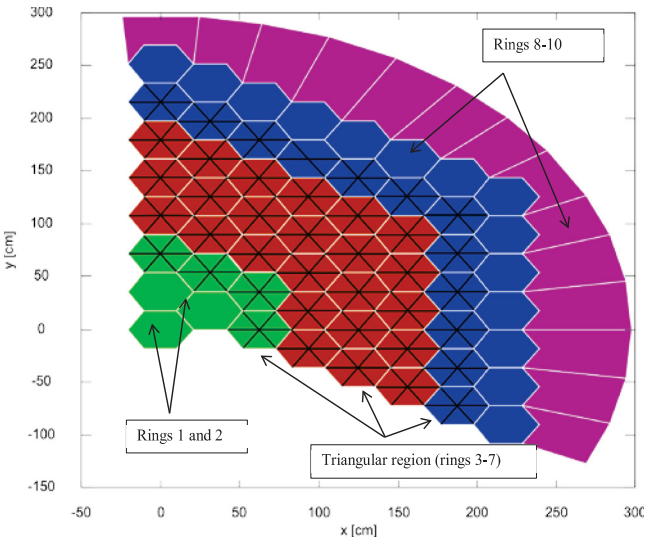

Fig. 8. Ring and triangular geometry utilized in the block model.

For the kinetic zone coupling between INSTANT and RELAP5-3D it was initially envisaged to couple the triangular feedback elements on a one-to-one basis, i.e., one triangular node in REALAP5-3D would provide temperature data to a triangular node in INSTANT, which would then pass back the triangular power distribution to RELAP5-3D for the next iteration. Since the modeling of the full MHTGR-350 core graphite structures in a triangular geometry requires 7,644 kinetic nodes (91 blocks on 14 layers with six triangles each), a full core triangular model was not an option due the limitations in the number of kinetic zones available in RELAP5-3D. (There are in fact 7644*2=15288 nodes required if the fuel and moderator temperatures were to be resolved separately). On the neutronics side of the coupling, INSTANT therefore uses a hexagonal mesh for the neutronics solution corresponding to a fuel or reflector block, corresponding to a single flux or power value per block.

III.C. Model Size and Computational Performance

As can be expected, the increase in model resolution and subsequent larger temperature and power datasets resulted in significant penalties in terms of model size and computational performance. A comparison of the two PHISICS/RELAP5-3D models is presented in Table II. The RELAP5-3D run time of a typical converged steady-state solution for the thermal fluids standalone Ex. 2 increased from 0.1 h (ring model) to 5 h (block model). For Ex. 3, the coupled PHISICS/RELAP5-3D solution required 11 h to converge for the ring model, and 20 h for the block model. The run time for Ex. 3 includes the use of 28 parallel processors, compared to a single processor for Ex. 2. The main question, as addressed in the subsequent sections, is therefore if this investment in model development, simulation time and post-processing lead to significant gains in the block model results, compared to the much simpler and faster ring model.

TABLE II

Comparison of ring and block model metrics.

Description	Ring model	Block model
Hydrodynamic components	~20	~250
Heat structures	~20	~1,100
Materials	9 (constant properties)	~100 (temperature and fluence dependent)
Kinetic feedback zones	170	~4,700
Radiation/conductio n enclosures	17 enclosures with ~350 surfaces	88 enclosures with ~7,000 surfaces
Decay heat treatment	1 table (global core power)	220 tables (block power)
Input file size (number of lines)	~30,000	~90,000
Real time required for converged steady state (hours)	*Ex. 2:* 0.1 *Ex. 3:* 11	*Ex.2*: 5 *Ex. 3:* 20

IV. EXERCISE 1 RESULTS

Exercise 1 of Phase I require a neutronics-only steady state solution for the MTHGR core. Fixed macroscopic cross sections are provided in 26 groups for each of the 22 fuel assemblies on the 10 core axial levels, as well as reflector cross section sets. INSTANT in stand-alone mode has been used to solve this problem using both the hexagonal (block) and triangular spatial resolution, since the cross-section data is defined at constant temperatures and no feedback is required.

The eigenvalue results for three control rod (CR) positions are compared in Table III: nominal (rods inserted 79.3 cm), fully inserted (bottom of active core) and fully extracted (top of active core). All cases utilized P_1 transport

with first order surface and 3rd order source expansions. The 33 pcm difference between the hexagonal and triangular models for the "CR extracted" case can be attributed to the different methodologies implemented for the hexagonal and triangular solvers in INSTANT – the hexagonal solutions should approach the triangular solution is a sufficient spatial refinement is performed. Since the CRs are only inserted one axial level into the core for this MHTGR-350 state point, the differences in the two models for the nominal case is also minimal (50 pcm).

TABLE III

Ex. 1: Comparison of hexagonal and triangular INSTANT results.

INSTANT Model	CR extracted	CR nominal	CR inserted	CR Worth (delta k/k)
Hexagonal	1.06754	1.06694	1.05826	870
Triangular	1.06722	1.06645	1.05505	1,140
delta k	33	50	321	-

The largest difference of 321 pcm occurs when the "smeared" out hexagonal CRs region is inserted fully over the height of the core. This can be expected from the modeling approach, since the CRs region for the triangular model was only defined as a single triangle (region 234 in Fig. 9), whereas the CRs in the hexagonal model were homogenized over the entire block volume (region 232).

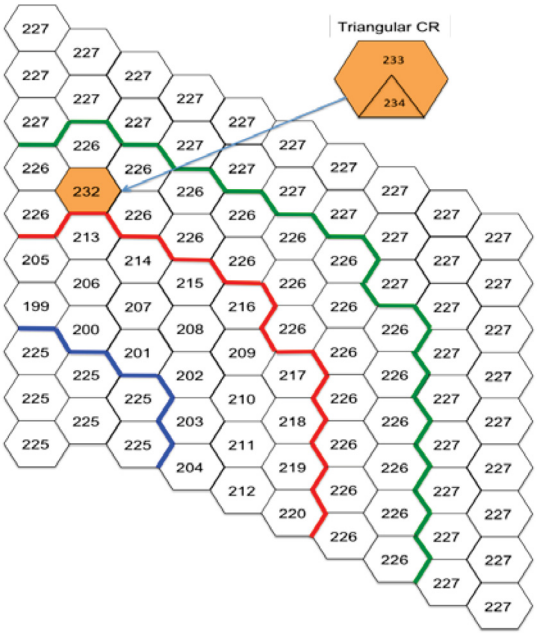

Fig.9. Whole core neutronics layout for Active Core Layer 10, with control rod location shown.

The active core power density distribution is presented in Fig. 10 and Fig. 11 for axial level 1 (core bottom) and level 7 (axial power peak location), respectively. The power generation in the fresh fuel blocks 9, 11 and 13 (see Fig. 3 for block numbering) in the inner fuel ring is significantly higher than the power densities in the depleted fuel blocks next to them, due to the MHTGR-350 core loading scheme. The radial variation in power density between fuel rings 1, 2 and 3 can also be observed in these two figures, with the 6 inner fuel blocks producing significantly more power than the central and outer fuel blocks. Similar differences can be observed in the Ex. 1 flux profiles of the 26 groups, but since this data is very similar to the Ex. 3 data, a few selected flux distributions are shown in section VI.

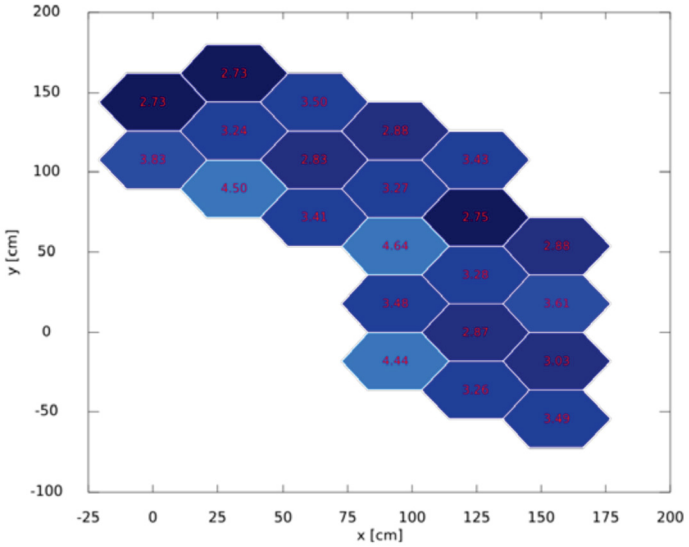

Fig. 10. Ex.1 – INSTANT power density (W/cm^3) distribution on Level 1 (bottom of core).

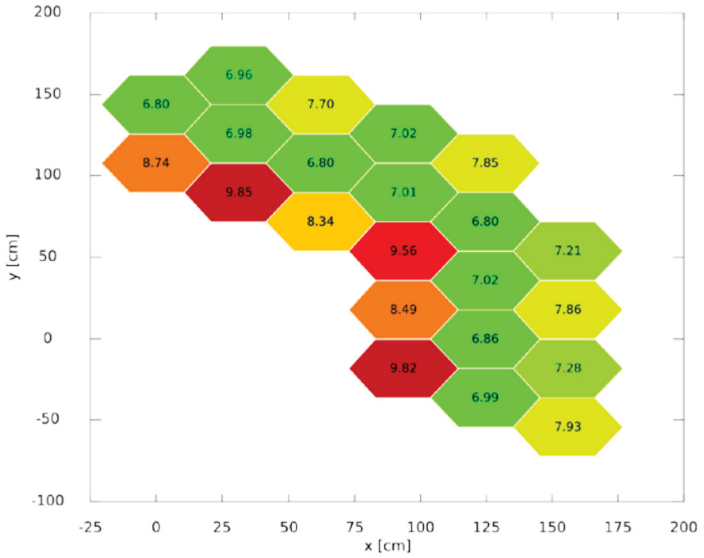

Fig. 11. Ex.1 – INSTANT power density (W/cm^3) distribution on Level 7 (location of axial peak power).

V. EXERCISE 2 RESULTS

RELAP5-3D in stand-alone mode has been used to solve the four sub-cases of Exercise 2, which are defined as thermal fluids standalone calculations with fixed power density profiles in the fuel region. The four sub-cases are defined in order of increasing complexity: Ex. 2a assumes that all coolant flow is through the core region, and only fixed thermophysical properties (e.g. thermal conductivity) are specified. For Ex. 2b, the bypass flow modeling in seven fixed bypass flow channels, totaling up to 11% of the total inlet flow rate, are required. Instead of the fixed thermophysical properties provided for Ex. 2a and Ex. 2b, the material properties prescribed for Ex. 2c vary as complex functions of fluence and temperature. The definition of Ex. 2d combines the variable material properties with the requirement to model the bypass flow distribution explicitly through the 2-mm gaps between the blocks.

The primary parameters of interest for Ex. 2 are the gas and solid temperatures and global parameters such as the pressure drop over the core and the inflow mass flow rate. The benchmark does however require participants to also report secondary parameters such as the calculated thermal conductivities, mass flow rate or velocities in bypass channels and heat transfer factors, since this data can be utilized to trace the source of possible differences in the primary parameters. In this paper, only a subset of the available data will be presented to illustrate the main characteristics for each of the exercises.

The Ex. 2a fuel temperature distributions shown in Fig. 12 (ring model) and Fig. 13 (block model) for the bottom core axial layer illustrate the increased spatial resolution of the block model over the ring model. A much more detailed distribution of temperatures was obtained on the triangular mesh compared to as few as three values per axial layer for the ring model. As can be expected from the volume-averaged approach in the ring model, all temperatures are significantly under-estimated compared to the block model values, which predicts significant radial temperature variations between the three fuel rings on this axial level (up to 300°C in Fig. 13).

The effect of the higher power generation in the fresh fuel blocks (as shown in Fig. 11 for Ex. 1) can be observed in the block model temperature distributions. The blocks with the highest power density (#9 and #13) also produce the highest fuel and graphite temperatures, as could be expected. This information is not available in the ring model, where the block power densities and temperatures are all averaged to one value per ring only.

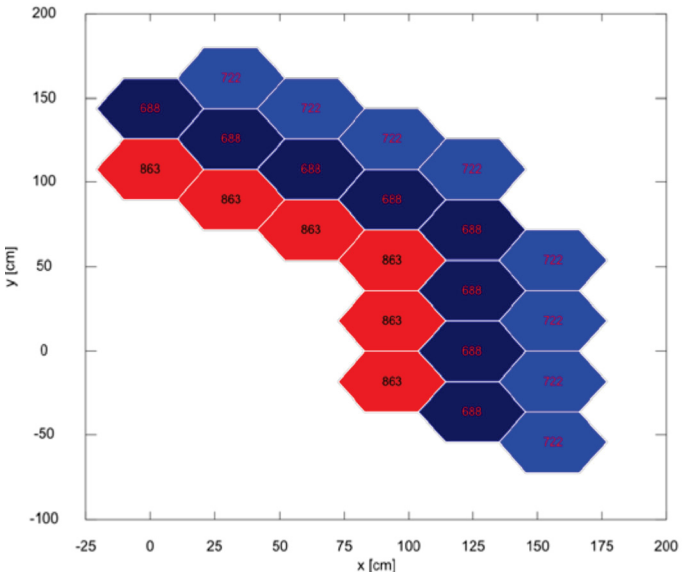

Fig. 12. Ex. 2a – Average fuel temperature (°C) distribution on axial Level 1 (first bottom core level) for the ring model.

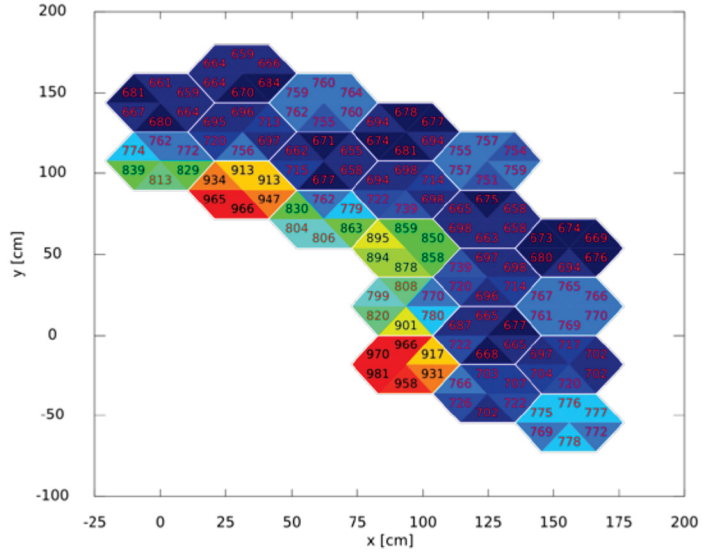

Fig. 13. Ex. 2a – Average fuel temperature (°C) distribution on axial Level 1 (first bottom core level) for the block model.

The graphite temperature distribution is shown for the whole core region in Fig. 14 (ring model) and Fig. 15 (block model). The relatively high inner reflector temperatures can be seen in both figures, since Ex. 2a did not include any bypass flow modeling in the reflectors. The block model (Fig. 15) show six equal values in the regions where a ring representation is used, e.g. blocks 1 and 2, but the detailed information available form this model is again apparent in the triangular regions of the core.

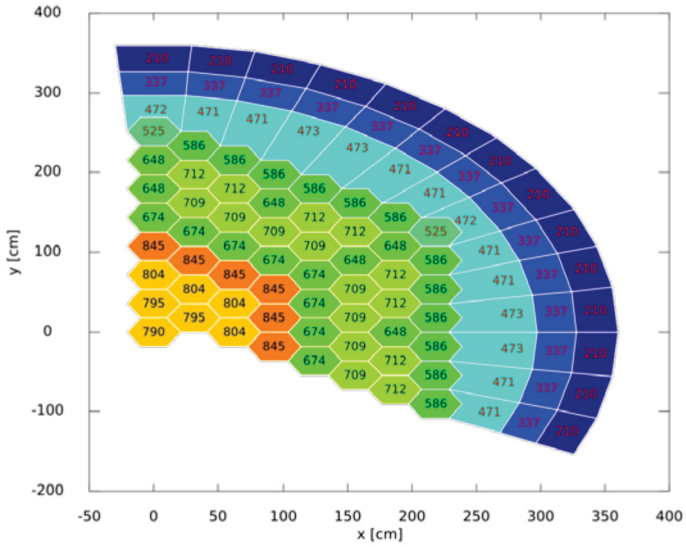

Fig.14. Ex. 2a – Average graphite temperature (°C) distribution for all graphite structures in the ring model on axial level 1 (first bottom core level).

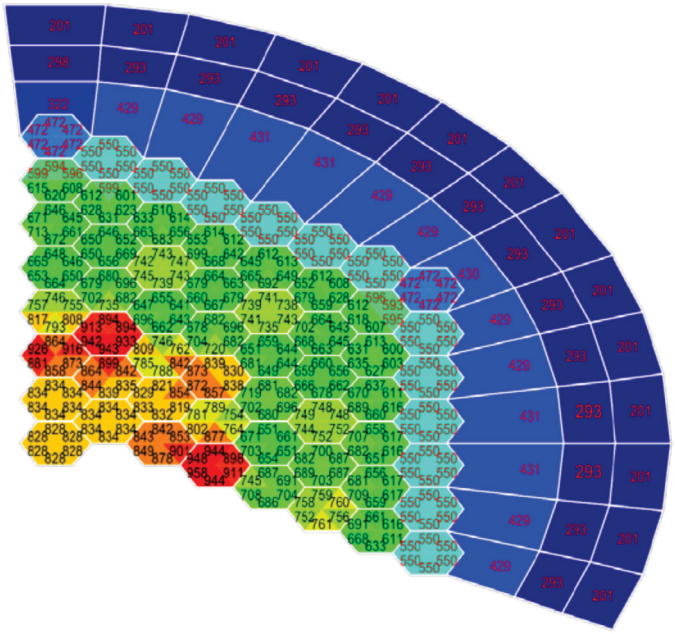

Fig. 15. Ex. 2a – Average graphite temperature (°C) distribution for all graphite structures in the block model on axial level 1 (first bottom core level).

As an example of the data that can be obtained from the detailed block model, the average fuel temperature axial profiles for the six triangular elements of block 9 are presented in Fig. 16. The block 9 average value can then be calculated from this data, and compared with the inner fuel ring temperature result obtained from the ring model, as shown in Fig. 16. The typical under-prediction of the ring model is again apparent in this axial temperature profile.

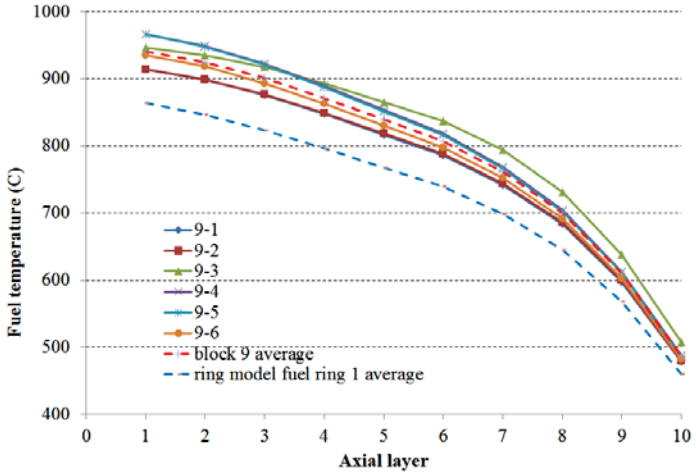

Fig.16. Ex. 2a – Block 9 triangular element average fuel temperatures (°C).

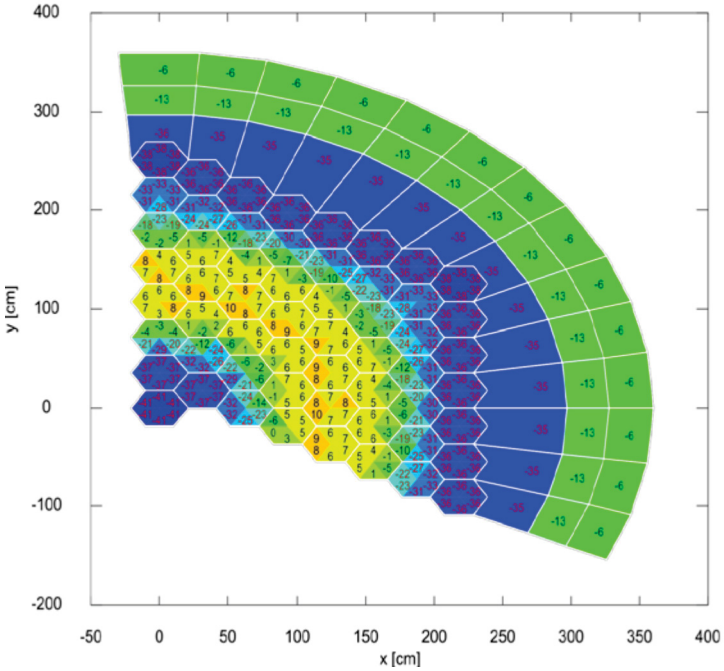

Fig.17. Average graphite temperature difference (%) between Ex. 2a and Ex. 2b for all graphite structures in the block model on axial level 1 (first bottom core level).

The inclusion of the 11% bypass flow in the Ex. 2b RELAP5-3D model leads to significant decreases in the inner and outer graphite reflector temperatures, as shown in Fig. 17. The block model predicts up to 41% lower temperatures in the inner reflector region. The effect on the fuel region is in the opposite direction (i.e., Ex. 2b exhibits higher fuel temperatures), but this difference is comparatively small (less than 10%). This is because a decrease from 100% to 89% of the nominal helium flow rate through the core still represents a very effective convective heat removal mechanism.

It should be noted that Ex. 2b represents an unphysical MHTGR-350 scenario, since approximately 6% of all energy is deposited outside the fuel region in the reflectors via fast neutron and gamma interactions [8]. This non-local heat deposition is not included in the benchmark specification, and will lead to much higher reflector temperatures, which will counter the effects of these reflector bypass flows to some degree.

The only difference between Ex. 2b and Ex. 2c is the addition of the variable thermophysical properties. The RELAP5-3D MHTGR-350 benchmark model for Ex. 2c uses a number of additional graphite materials to account for the fluence dependent thermophysical properties, as prescribed in the benchmark specification. The proper modeling of the decrease in thermal conductivity with an increase in fast flux exposure is especially important for fuel and graphite temperatures during the loss of cooling transients in Phase II. Only minor differences are observed between these two Phase I cases, since the convective heat transport of the active helium cooling during normal operation dominates the effects of changes in the material conductivity and specific heat. The difference between Ex. 2b and Ex. 2c will become more significant during the loss of cooling transients that will be performed for Phase II.

Exercise 2d combines the effects of bypass flows and variable thermophysical properties. The difference between Ex. 2c and Ex. 2d is the specification that the real geometry of the MHTGR-350 must be used to determine the converged bypass flows in the 2 mm gaps that exist between all blocks, as well as the 3.5 mm gap between the outer reflector and the CB. This exercise is designed to capture the high resolution and fidelity that Computational Fluid Dynamics (CFD) is capable of, but since the intended design use of RELAP5-3D is typically thermal system analysis of a lower fidelity, the current RELAP5-3D model can only approximately the real geometry of these gaps with a network of 1D pipe elements. The RELAP5-3D block model predicts a total of 14.2% bypass flow outside the core region, i.e. 3.2% more than the fixed values used in Ex. 2b and Ex. 2c. The bypass flow differences between Ex. 2c and Ex. 2d are small enough that the relative fuel temperature data of the respective block models differ by less than 4%, as shown in Fig. 18.

VI. EXERCISE 3 RESULTS

Exercise 3 combines the solutions of the neutronics and thermal fluid domains, and therefore requires the use of a coupled solution methodology. For Ex. 3a, the PHISICS/RELAP5-3D model is created by combining the RELAP5-3D standalone thermal fluid model developed for Ex. 2c (11% bypass flow, variable thermophysical properties) with a RELAP5-3D kinetics section that defines the mapping to cross-section data contained in the temperature and xenon-135 dependent library *lib.xml*.

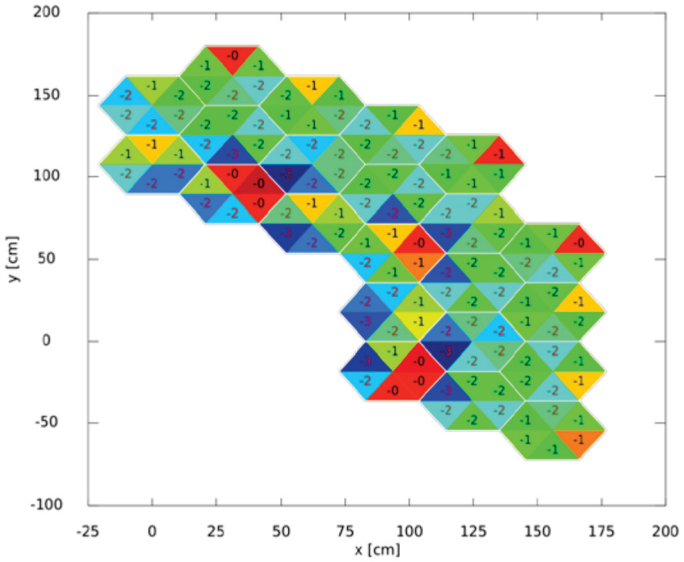

Fig.18. Average fuel temperature difference (%) between Ex. 2c and Ex. 2d on Axial Level 1 (first bottom core level) for the block model.

The only variation between Ex. 3a and Ex. 3b occurs in the definition of the bypass flows, i.e. Ex. 2c forms the thermal fluid basis model for Ex. 3a and Ex. 2d is used as the basis for Ex. 3b.

As a first step in the PHISICS/RELAP5-3D (PR5) solver scheme, the xenon equilibrium is obtained by using MRTAU to “burn” the core in 4 time steps of 2.5 days each, i.e. for a total of 10 days. This process involves four recalculations of the flux with INSTANT after every 2.5 days. During the depletion phase, the fuel and reflector temperatures for the cross-section evaluation are kept constant. For each flux recalculation with INSTANT, the macroscopic cross-section sets are first interpolated for the new xenon density. The new xenon absorption contribution for each node is then calculated with the updated xenon density and added to the macroscopic cross-section sets. Since the core is only burned for a very small duration, the assumption that all the material number densities apart from xenon remain constant is acceptable. Once xenon equilibrium is reached, RELAP5-3D iterates with INSTANT to obtain a converged temperature field for this xenon distribution. After this initial MRTAU-INSTANT-RELAP5-3D iteration, MRTAU burns the core again for 2.5 days to find the new xenon equilibrium corresponding to the new temperature distribution.

A comparison between the eigenvalues and CR worths obtained for Ex. 3a and Ex. 3b is summarized in Table IV for the ring and block models. (This data cannot be compared with the data presented for Ex. 1 in Table III, since the two exercises use two different libraries and are calculated at significantly different state points).

TABLE IV

Ex. 3a and Ex. 3b: Comparison of PHISICS/RELAP5-3D keff and CRs worths for ring and block models.

PHISICS-RELAP5-3D model	CR nominal	CR all out	CR all in	CR worth delta k/k (pcm)
3a				
ring	1.03447	1.03593	1.02673	888
block	1.03394	1.03511	1.02513	965
delta k	*53*	*81*	*160*	
3b				
ring	1.03336	1.03450	1.02493	926
block	1.03384	1.03503	1.02549	922
delta k	*-48*	*-52*	*-56*	

For Ex. 3a, the difference between the ring and block models are relatively small (less than 160 pcm), and the largest difference is again observed for the all rods inserted case. The predicted CR worths are within 80 pcm for the two models. A slightly different pattern is observed for Ex. 3b, where the block eigenvalues are less than the ring model values and the two CR worths are almost identical. The only differences between the two cases are the changes in the fuel (Doppler) and moderator temperatures due to the slight variation in the bypass flow distribution, which act as the drivers for the small variances predicted for the two exercises.

The power density distribution reaches a maximum axial value on level 8 (634 cm from the bottom of the core). As an example, the power density distribution is shown for Ex. 3a in Fig. 18, where a peak value of 11 W/cm^3 is calculated in block 13. (The power and flux data are calculated on the hexagonal mesh, as explained in section III.B).

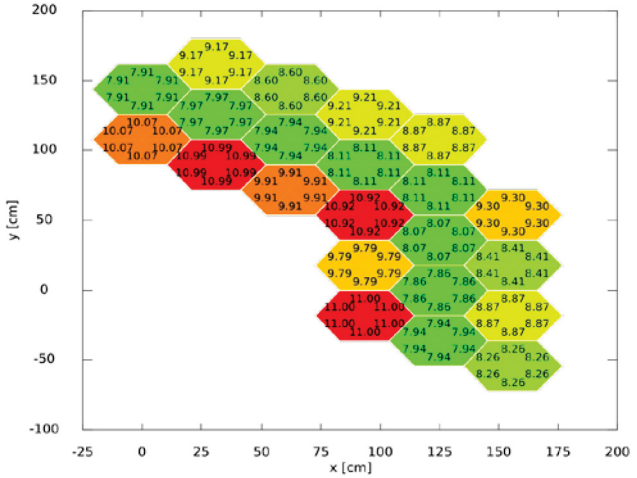

Fig. 18. Ex. 3a - Power density (W/cm^3) distribution on axial Level 8 for the block model.

Two fast and thermal flux data examples are shown in Fig. 19 and Fig. 20 for two of the 26 groups. The Ex. 3a data shown here was taken at axial level 8 where the axial flux profiles reach a maximum value. The fast flux peak in the fuel regions of the core is clearly visible in Group 1 (Fig. 19), whereas the peak thermal flux occurs in Group 20 and in the inner reflector as the fast neutrons are thermalized (Fig. 20).

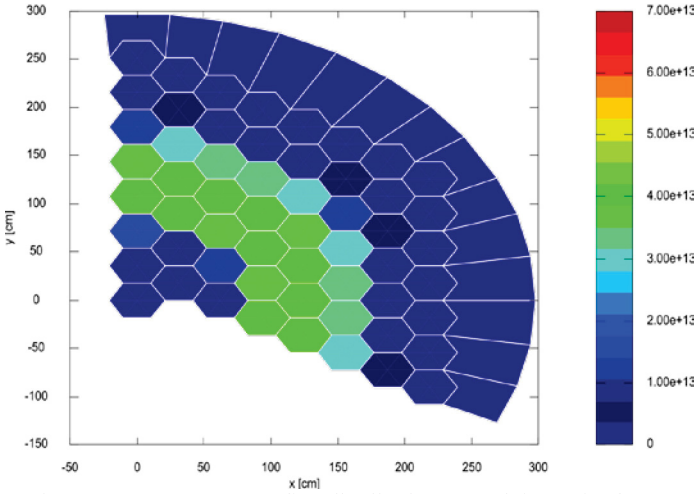

Fig. 19. Ex. 3a – Group 1 flux distribution on Axial Level 8 for the block model (fast peak value).

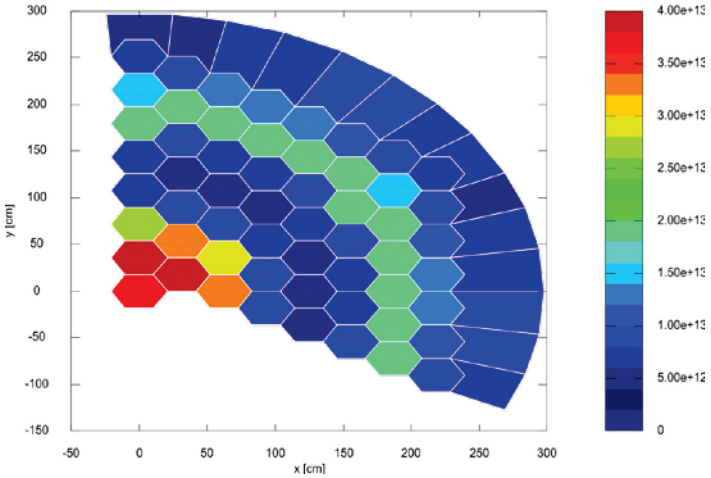

Fig. 20. Ex. 3a – Group 20 flux distribution on Axial Level 8 for the block model (thermal peak value).

As a final example, the average fuel temperature relative difference (%) between Ex. 2d and Ex. 3b is shown for the bottom (Fig. 21) and top (Fig. 22) axial layers of the core. In the hot bottom regions of the core the differences are less than -8% (i.e. the temperatures are higher for Ex. 2d than Ex. 3b), but these variations increase as the colder upper regions of the core are reached, where differences up to 23% is calculated for block 29 (Fig. 22).

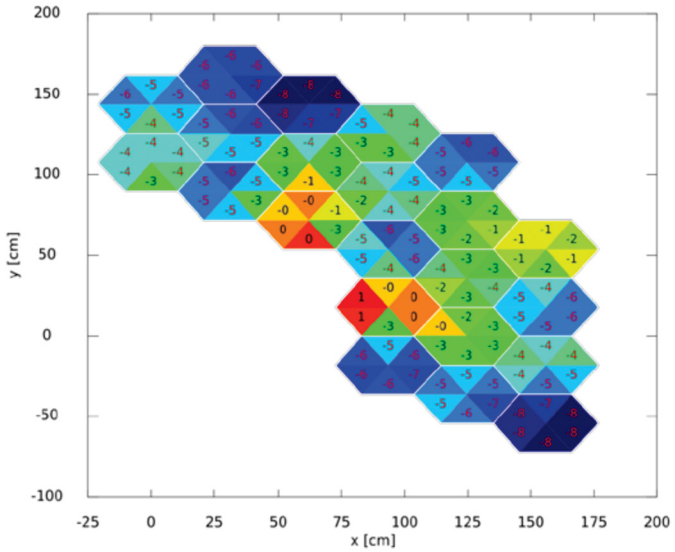

Fig. 21. Average fuel temperature difference (%) between Ex. 2d and Ex. 3b on Axial level 1 (first bottom core level) for the block model.

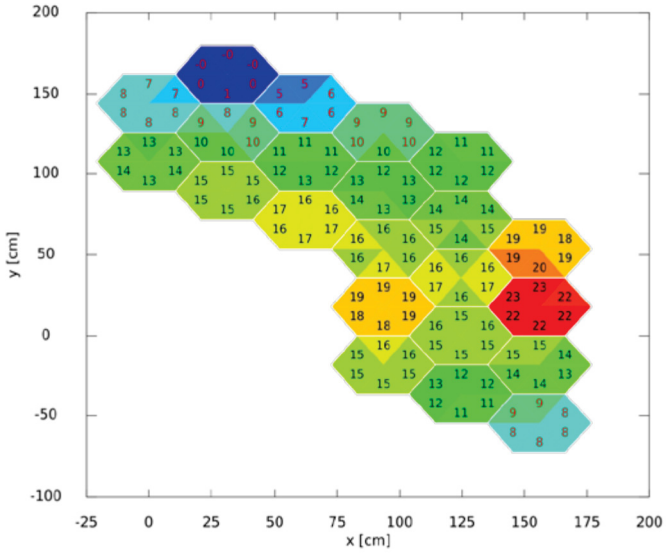

Fig. 22. Average fuel temperature difference (%) between Ex. 2d and Ex. 3b on Axial level 10 (top of core) for the block model.

A significant difference therefore exists between the axial temperature profiles of Ex. 2c and Ex. 3b (shown in Fig. 23 for block 9, as an example). This is caused by the feedback kinetics of the coupled case, as opposed to the constant power profile specified in Ex. 2d. The cross-section feedbacks on the xenon concentration, control rod position and the fuel and moderator temperatures all contribute to this change in the axial temperature distribution.

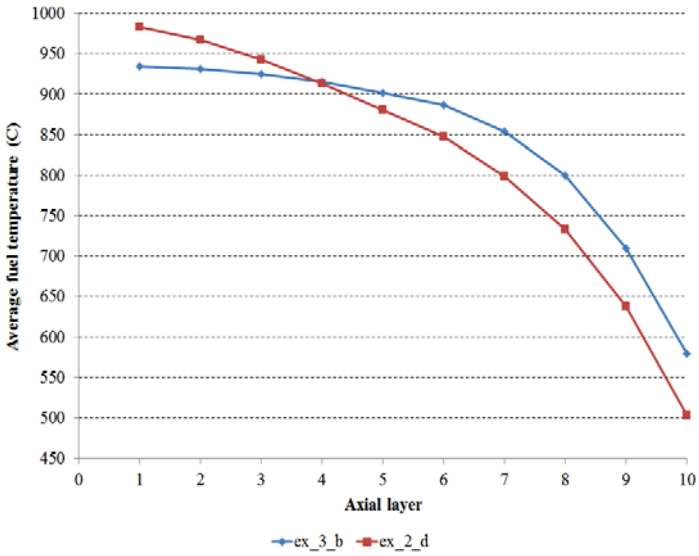

Fig. 23. Comparison of Block 9 axial average fuel temperature profiles for Ex. 2d and Ex. 3b.

IV. CONCLUSIONS

The summarized INL results for Phase I of the OECD/NEA MHTGR-350 benchmark were presented for two models: a conventional homogenized "ring" model and a much more detailed triangular-based "block" model. It has been showed that the RELAP5-3D code, primarily developed for system thermal analysis, can be applied to obtain much more detailed fuel and reflector temperature profiles in a prismatic HTGR core. Although a significant penalty was paid in terms of the computational resources required, the resultant gain in spatial fidelity has been shown to be sufficient to warrant the development of such detailed models. The typical homogenized ring model approach followed by most system code model developers lead to a under-estimation of the MHTGR-350 fuel and reflector temperatures by as much as 10%, which could be an important factor in safety calculations for HTGR systems. The identification of possible power peaking and hot spots in the core further supports the conclusion of this study that the implementation of more detailed spatial models in coupled HTGR core analyses is worth the time and effort.

The MHTGR-350 benchmark proved to be a challenging simulation set of problems to model accurately, and even with the simplifications introduced in the benchmark specification this activity is an important step in the code-to-code verification of modern prismatic VHTR codes. A final OECD/NEA comparison report and combined journal publication will compare the Phase I and III results of all international participants in 2014, while the Phase II transient case results will be reported in 2015.

ACKNOWLEDGMENTS

This work was supported by the U.S. Department of Energy, Assistant Secretary for the Office of Nuclear Energy, under DOE Idaho Operations Office Contract DE-AC07-05ID14517.

The earlier contributions of Dr. Aaron Epiney (PSI, Switzerland) on the code and model development activities of this work are greatly appreciated.

REFERENCES

1. J. ORTENSI, et al., "Prismatic Core Coupled Transient Benchmark", *Trans. of the ANS* 104, p. 854 (2011).
2. G. STRYDOM, A. Epiney, "Relap5-3D results for Phase I (Exercise 2) of the OECD/NEA MHTGR-350 MW benchmark", *Proc. of ICAPP2012,* Chicago, USA (2012).
3. A. EPINEY, et al., "New Multi-group Transport Neutronics (PHISICS) Capabilities for RELAP5-3D and its Application to Phase I of the OECD/NEA MHTGR-350 MW Benchmark", *Proc. of HTR2012,* Tokyo, Japan (2012).
4. RELAP5-3D© Code Manual, Vol.1-5, Rev. 3, INEEL-EXT-98-00834 (2009).
5. A. EPINEY, et al., "PHISICS Multi-group Transport Neutronic Capabilities for RELAP5", *Proc. of ICAPP'12*, Chicago, USA (2012).
6. Y. WANG, C. Rabiti, G. Palmiotti, "Krylov Solvers Preconditioned with the Low-Order Red-Black Algorithm for the PN Hybrid FEM for the INSTANT Code," *Proc. of M&C 2011*, Rio de Janeiro, Brazil (2011).
7. A. ALFONSI, et al., "PHISICS Toolkit: Multi-reactor Transmutation Analysis Utility– MRTAU", *Proc. of PHYSOR 2012*, Knoxville, USA (2012).
8. G. STRYDOM, "TINTE uncertainty analysis of the maximum fuel temperature during a DLOFC event for the 400 MW Pebble Bed Modular Reactor", *Proc. of ICAPP 2004*, Pittsburgh, USA (2004).